COMBINATION OF IMMOBILIZED TiO_2 AND ZERO VALENT IRON FOR EFFICIENT ARSENIC REMOVAL IN AQUEOUS SOLUTIONS

J.M. Raez[a], A. Arencibia[b], Y. Segura[a], J.M. Arsuaga[c], M.J. López-Muñoz[a,*]

[a]Departamento de Tecnología Química y Ambiental, [b]Departamento de Tecnología Química, Energética y Mecánica, [c]Departamento de Ciencias de la Educación, Lenguaje, Cultura y Artes, Ciencias Histórico-Jurídicas y Humanísticas y Lenguas Modernas,

Universidad Rey Juan Carlos, C/ Tulipán s/n 28933 Móstoles. Madrid. Spain

*Corresponding author. Tel.: +34 916647464;

E-mail address: mariajose.lopez@urjc.es (M.J. López-Muñoz).

Abstract

The photocatalytic removal of arsenic from aqueous solutions was investigated using titania (TiO_2) immobilized on a glass support, both bare and combined with synthesized metallic iron nanoparticles (nZVI) or commercial microscale iron (ZVI). Three procedures, namely dip coating, rotational coating and sponge coating, were tested for achieving the immobilization of TiO_2. The photocatalytic activity of the semiconductor films under UV-irradiation after cumulative coatings was evaluated for 10 $mg \cdot L^{-1}$ aqueous As(III), which was completely oxidized to As(V) with all settings within 90 and 180 min. Titania immobilized by dip coating was found to be the most effective as it showed the faster kinetics. The reuse of immobilized TiO_2 was also investigated, detecting no changes in the photocatalytic activity after five consecutive reactions. The addition of commercial ZVI particles to the immobilized TiO_2 system did not bring about significant changes in the kinetics for As(III) oxidation at the three pH values investigated, i.e., 5, 7 and 9. On the contrary, by addition of nZVI not only a faster depletion of As(III) was attained

in comparison to bare titania but also the removal of As(V) from the solution to concentrations below that recommended by the World Health Organization for human consume (10 μg L^{-1}), indicating this system can be suitable for the treatment of water polluted with arsenic.

The role of iron species in the arsenic removal process with both [ZVI+immobilized-TiO_2] and [nZVI+immobilized-TiO_2] systems was further investigated by performing adsorption and irradiation experiments without titania. It was inferred that within the pH range evaluated, the minor corrosion of the ZVI surface even under UV irradiation restricts the production of reactive oxidizing species and generation of sites for As(III) and/or As(V) adsorption. By contrast, adsorption should be the main process responsible for the overall diminution of As(III) and As(V) species in solution attained upon nZVI addition, promoted by the increase of the external oxides/hydroxides layer on iron nanoparticles. Nevertheless, a certain contribution of UV-generated oxidant species to the photocatalytic oxidation performance of titania might also be considered.

Keywords

Arsenic removal, TiO_2 immobilization, ZVI nanoparticles, photocatalytic oxidation, As-adsorption

1. Introduction

The presence of arsenic in drinking water is a potential threat to human health. The exposition to this element causes toxic effects and is associated with brain, bladder, liver, kidney, and skin cancers (WHO, 2017; WHO, 2001; Jomova et. al., 2011; Shankar et al., 2014; Abdul et al., 2015). Inorganic and organic arsenic are naturally present in water, being inorganic forms the most abundant and hazardous. In aqueous systems, arsenic primarily exists as oxyanions of trivalent arsenite, As(III), or pentavalent arsenate, As(V). Since arsenite is more toxic, mobile, and difficult to remove than arsenate oxidation processes are usually applied as a pre-treatment to enhance the overall arsenic removal efficiency (Sharma and Sohn, 2009; Sorlini and Gialdini, 2010).

Although conventional chemical oxidation has been customarily applied to transform As(III) to As(V) (Sorlini and Gialdini, 2010), heterogeneous photocatalysis with titanium dioxide (TiO_2) can be a good alternative as it has been proven to be able to achieve the complete oxidation of As(III) to As(V) in aqueous solution (Dutta et al., 2015; Ferguson et al., 2005; Choi et al., 2010; Yoon et al., 2009; López-Muñoz et al., 2015). Once the As(V) species are generated, however, the adsorption capacity of TiO_2 for them is very low thus resulting in an inefficient removal of the arsenate formed. For this reason, in order to attain the complete elimination of arsenic in one stage, the addition of a suitable adsorbent with high adsorption ability for As(V) under photo-irradiation would be required (Yu et al., 2013). One plausible option is the use of microscale zero valent iron (ZVI) and nanoscale ZVI (nZVI) since over the last years both species have been successfully applied as adsorbents for the treatment of water polluted with arsenic (Su and Puls, 2001; Morgada et al., 2009; Bhowmick et al., 2014; Bhaumik et al., 2015).

In this regard, we reported in a previous work (López-Muñoz et al., 2017) that the combination of heterogeneous photocatalysis with TiO_2 and powdered zero-valent iron (ZVI) showed a synergic effect in the oxidation of As(III) and subsequent adsorption of As(V) generated. The UV-irradiation of a 10 mg L^{-1} As(III) aqueous solution at pH 3 in the presence of titania (0.25 g L^{-1}) and metallic iron (0.1 g L^{-1}) led to a final concentration of total arsenic in solution well below the maximum value recommended by the World Health Organization (WHO) in drinking water (10 μg L^{-1}) (WHO, 2001). The beneficial contribution of ZVI particles was mainly explained by the oxidation of the iron surface to different stable iron hydroxides/oxides able not only to retain arsenic species but also to generate reactive oxygen species (ROS) (López-Muñoz et al., 2017).

With the objective of a practical application, however, one important shortcoming of the above system was the use of a slurry reactor. The slurry operation has significant advantages among which a high ratio of irradiated photocatalyst surface to the effective reactor volume, a rather uniform distribution of the suspended catalyst, and scarce mass-transfer limitations. These benefits make slurry reactors with suspended titania particles the most widely employed for research purposes. On the other hand, slurry systems have also several drawbacks that prevent

their use in large scale applications, such as the costs to remove the TiO_2 particles from the effluent after the treatment, the aggregation of suspended particles at high catalyst loads and the difficulty for being applied to continuous flow systems (Manassero et al., 2017; Marugán et al., 2016). Such shortcomings can be overcome by using reactors with immobilized TiO_2 so that no separation of the catalyst particles is needed, also improving the reutilization of the catalyst in consecutive cycles. Nevertheless, compared to slurry operation mode, immobilized systems show a lower accessibility of the catalyst to photons, and a low area-to-volume ratio which can lead to mass transfer limitations and low reaction rates (Balasubramanian et al., 2004; El-Kalliny et al., 2014; Singh et al., 2013; Chen et al., 2001). Accordingly, the rate of the reaction and the pollutant transformation achieved will be significantly affected by the thickness of the layer of immobilized catalyst, since it governs the extent of radiation that can be absorbed and also the limitations of access to the photocatalyst close to the support due to the internal mass transfer (Vezzoli et al., 2013).

Different physical and chemical procedures leading to the TiO_2 immobilization over diverse supports have been specifically proposed for photocatalytic treatments. Among others, it should be mentioned spread coating and dip-coating, chemical vapour deposition, pulsed laser deposition or electrospray (Shan et al., 2010). Particularly, the dip-coating method has been widely used for the immobilization of TiO_2 because the resulting coatings exhibit suitable uniformity and stability. In this procedure, the support is immersed into a titania solution and then withdrawn with controlled speed. The thickness of the immobilized layer depends on the withdrawal speed, the properties of the immersion solution, and the number of coatings (Dijkstra et al., 2001; van Grieken et al., 2009; Falk et al., 2018). Glass supports have been preferably employed for the immobilization of TiO_2 by dip-coating due to their high light transparency and resistance to calcination (Shan et al., 2010).

In this context, the first objective of the present investigation was to evaluate the photocatalytic performance of immobilized titania for the treatment of water polluted with arsenic. With this aim, we compared different procedures for the immobilization of TiO_2 on glass by modifying the

104 method of impregnation and the number of coatings. The photocatalytic activity as well as the
105 stability after consecutive reuse cycles was analysed for each system. The second objective was
106 to investigate the influence of zero-valent iron addition to the immobilized TiO_2 system on the
107 overall arsenic removal. Two materials were evaluated, i.e. commercial microscale metallic iron
108 (ZVI) and synthetized nanoscale iron (nZVI). The influence of pH was studied in the range 5-9
109 avoiding strong acidic pH values to prevent the iron leaching to the solution.

110 ## 2. Experimental

111 ### 2.1. Chemicals

112 The stock As(III) and As(V) solutions were prepared from $NaAsO_2$ and $NaAsO_3$ (90%, Aldrich),
113 respectively. Titanium dioxide (Degussa P25) and commercial ZVI powder (97%) were provided
114 by Evonik and Aldrich, respectively. For the synthesis of iron nano-particles : $FeSO_4 \cdot 7H_2O$
115 (>99%, Sigma Aldrich) as iron source, ethanol (>99%, Scharlab), NaOH (>98%, Aldrich), and
116 $NaBH_4$ (>98%, Sigma Aldrich) were used. Isopropanol (99.5%) and potassium hydroxide (90%)
117 employed for the pre-treatment and cleaning of glass tubes were supplied by Scharlab. For pH
118 modification, HCl (37%, Sigma Aldrich) was used.

119 ### 2.2. Synthesis of nZVI

120 Metallic iron nano-particles (nZVI) were synthesized according to a modified method described
121 elsewhere (Ponder et al., 2000). First, a solution of $FeSO_4 \cdot 7H_2O$ 0.4 M in ultrapure water and
122 ethanol (70:30 v/v) was sonicated for 2 hours. In absence of oxygen, the pH of solution was
123 adjusted to 6.8 with NaOH 3.8 M. Then, an excess of $NaBH_4$ was added to the mixture to reduce
124 Fe(II) to Fe(0). The metallic iron was washed with a solution of water and ethanol (50:50 v/v),
125 and subsequently treated with pure ethanol to complete the removal of water and avoid the iron
126 oxidation. Finally, the solid material was recovered by filtration and dried under vacuum.

127 ### 2.3. Procedures for the immobilization of TIO_2

128 A borosilicate glass hollow cylinder (235x60 mm) with one closed side was used as support for

129 titania immobilization. Initially, the glass cylinder was immersed into a KOH/isopropanol (0.5
130 M) solution for 24 hours in order to attain a net negative charge on the glass walls. Afterwards, it
131 was washed with ultrapure water and dried at 110 °C.

132 The immobilization of TiO_2 was carried out by three different methods: dip coating (DC),
133 rotational coating (RC), and sponge coating (SC). For each procedure it was employed an aqueous
134 suspension of 200 g TiO_2 L^{-1} at pH = 2 (adjusted with HCl 3 M) thus favoring the interaction of
135 positively charged titania particles with the borosilicate glass support (van Grieken et al., 2009).
136 In the dip coating method, the glass support was immersed vertically into the suspension for 5
137 min at a controlled immersion speed of 2 $mm \cdot s^{-1}$ and pulled out at a withdrawing rate of 1
138 $mm \cdot s^{-1}$. The rotational method was performed by dipping horizontally one eighth of the glass
139 support into the TiO_2 solution turning on its axis at a rotation speed of 9 $° \cdot s^{-1}$ for two min. Finally,
140 the sponge coating method consisted in manually soaking the support with the TiO_2 suspension
141 by means of a porous sponge. After coating, all supports were carefully dried at 110 °C for 20 h
142 and calcined at 550 °C for 2 h (heating ramp $5° \cdot C\ min^{-1}$). Three coating cycles were carried out
143 for each immobilization method. The quantification of the TiO_2 catalyst successfully deposited
144 was determined by the mass difference between the glass support before and after titania
145 impregnation. An estimation of the average TiO_2 thickness was calculated taking a value of 3.7 g
146 cm^{-1} for density of titania (Chen and Dionysiou, 2006).

147 **2.4. Characterization Techniques**

148 XRD patterns of iron materials were recorded on a Philips X-PERT MPD diffractometer using
149 Cu Kα radiation, in the range of 5 to 90 degrees. Transmission Electron Microscopy (TEM)
150 images of nZVI, Energy-Dispersive X-ray (EDX) microanalysis, and electron diffraction analysis
151 were carried out in a PHILIPS TECHNAI 20 T microscope operating at 200 kV. The particles of
152 nZVI were dropped on an ultrathin carbon film-coated Cu grid after being dispersed in acetone.
153 The size of iron particles was determined by the analysis of TEM images with the Image-J®
154 software.

Temperature-programmed reduction (TPR) analysis was conducted on a Micrometritics Autochem 2910 equipment. The TPR profiles of the samples were recorded between 100 and 900 °C in presence of a H_2/Ar mixture (10/90% v/v) flowing at 40 mL min^{-1}, at a heating rate of 10 °C min^{-1}. N_2 adsorption-desorption isotherms were acquired at 77 K with a Micromeritics Tristar 3000 analyser, using two sequential degasification steps, performed at 363 K and 373 K under nitrogen. The Brunauer–Emmett–Teller model was used to estimate the specific surface area (S_{BET}) of TiO_2 and iron particles (Brunauer et al., 1938).

2.5. Photocatalytic reactions

A cylindrical reactor of 1 L effective volume open to the atmosphere was used for the batch photocatalytic reactions. The initial concentration of As(III) in solution was fixed at 10 mg L^{-1}. Prior and during the photocatalytic runs, the solution was aerated (air flow rate of 0.1 L min^{-1}) and magnetically homogenized (750 rpm). Aliquots were taken at selected times for the measurement of arsenic concentration. For the irradiation, a medium-pressure mercury lamp (Heraeus TQ-150) was placed concentrically within the borosilicate glass hollow cylinder with the immobilized TiO_2, and the whole set was axially immersed into the aqueous solution.

The colorimetric determination of the concentration of As(III) and As(V) in the range 1 to 10 mg·L^{-1} was performed on a Jenway 7300 spectrometer, following the formation of a complex between arsenic and molybdate as described elsewhere (López-Muñoz et al., 2015). For arsenic concentrations lower than 1 mg L^{-1} an atomic fluorescence spectrometer working by hydride generation (HG-AFS) (PSA 10.055 Millenium Excalibur) was employed. The separation of As(III) and As(V) species was attained by HPLC (SpectraSYSTEM P1000) using a strong anion exchange column (Hamilton PRP-X100). Error analysis was carried out by propagation of uncertainty estimating the instrumental error for each arsenic concentration. Error bars are included in the kinetic profiles. To assess the reproducibility of the experimental results, the reactions were repeated three times. In agreement with the instrumental error, the values of relative standard deviation (RSD) of the arsenic concentration in the aqueous solution were smaller than 10% in all cases.

3. Results and discussion

3.1. TiO_2 immobilization for As(III) oxidation

The influence of the immobilization method (i.e. DC, RC, and SC procedures) on the morphological properties of the layer of TiO_2 deposited on the glass cylinder was initially evaluated. With dip coating and rotational methods uniform and smooth coating layers were obtained. On the contrary, when the immobilization was attained by the sponge method the resulting layer presented small catalyst clusters regularly spread on the surface. As the number of coatings increased the surface of immobilized TiO_2 became slightly rougher, mainly in the rotational and sponge methods.

Table 1 summarizes the amount and average thickness of TiO_2 immobilized on the surface of the glass support determined for each procedure after consecutive coating cycles. Significant differences were observed depending on the method employed. After the first coating, the higher amount of immobilized TiO_2 was attained by using the SC method followed by rotational and vertical immersions, with 0.569, 0.512, and 0.272 mg of TiO_2 cm^{-2}, respectively. A similar trend was also observed for the subsequent coating cycles. In the case of the sponge method, the presence of small agglomerations over the continuous thin layer of immobilized TiO_2 might be responsible of the higher amount of supported catalyst as compared to the immersion methods. On the other hand, the larger amount of titania immobilized by the RC method in comparison to the DC method might be related to the experimental procedure used in each case. In the RC method the glass cylinder was partially immersed into the titania suspension while it was rotating, alternating immersion with exposure to air for 2 min. This should favor the ongoing deposition of a new thin layer of titania over that attained in the previous rotation thus leading to a higher amount of immobilized titania than obtained in the DC method.

205 **Table 1**. Mass and film thickness of TiO_2 immobilized after consecutive coating cycles

Number of coating cycles	Dip coating		Rotational coating		Sponge coating	
	Mass of TiO_2 (mg cm^{-2})	Average thickness (μm)	Mass of TiO_2 (mg cm^{-2})	Average thickness (μm)	Mass of TiO_2 (mg cm^{-2})	Average thickness (μm)
1	0.272	0.735	0.512	1.384	0.569	1.538
2	0.507	1.370	0.827	2.235	1.045	2.824
3	0.680	1.130	1.130	3.054	1.460	3.946

206

207 As seen in Table 1, the average thickness of TiO_2 immobilized significantly increased after each
208 coating cycle for the three methods following the order: dip coating < rotational coating < sponge
209 coating. Nevertheless, as the number of coatings increases a further away from a linear growth of
210 the mass of TiO_2 is observed. The additional amount of TiO_2 deposited after each coating steadily
211 diminished with the number of coating cycles. As compared to the first coating, the mass of
212 catalyst immobilized in the second and third cycles increased by 1.9 and 2.5-fold for the dip
213 coating; 1.6 and 2.2-fold for the horizontal rotational coating; and 1.8 and 2.6-fold for the sponge
214 coating, respectively.

215 **3.1.1. Photocatalytic efficiency of immobilized TiO_2**

216 The photocatalytic activity of TiO_2 immobilized by the three procedures was evaluated by the
217 oxidation of 10 $mg \cdot L^{-1}$ As(III) in aqueous solution at pH 9 (natural pH of the solution). Figure 1
218 displays the relative concentration of As(III) and As(V) species in the aqueous solution as a
219 function of the irradiation time.
220 As it can be seen, the removal of As(III) was achieved in all cases within 90 and 180 min of
221 irradiation. The best photocatalytic performance was detected for titania immobilized after the
222 first and second coating cycles by dip coating, completing the whole oxidation of As(III) to As(V)
223 after 90 min. The activity decreased, however, after the third coating cycle being necessary 120
224 min to accomplish the oxidation of As(III). Also 120 min were steadily required by the catalyst
225 immobilized by rotational coating to attain the complete oxidation of As(III) despite the similar
226 amount of titania deposited in comparison to that obtained after the second cycle with dip coating.

The sponge method of TiO_2 immobilization exhibited the worst efficiency in the oxidation since 180 min were necessary to reach the complete elimination of As(III). In general terms, the concentration profiles displayed in Figure 1 show that the activity of immobilized titania tapered off in the order dip coating> rotational coating> sponge coating.

The differences found must be related to the distribution of titania particles and thickness of the TiO_2 layer immobilized by each procedure. Previous studies have reported that the overall photocatalytic reaction rate in fixed-film reactors is influenced by the thickness of the catalyst film in a different way depending on the illumination configuration (Manassero et al., 2017). If the immobilized photocatalyst is irradiated from the solution-side in contact with the semiconductor, the reaction rate will increase with the thickness of photocatalyst until reaching a limit above which no further increase of photons absorption can take place. If that thickness is exceeded no enhancement of the photocatalytic reaction rate will occur with the increase of catalyst mass since the innermost layers will receive no radiation.

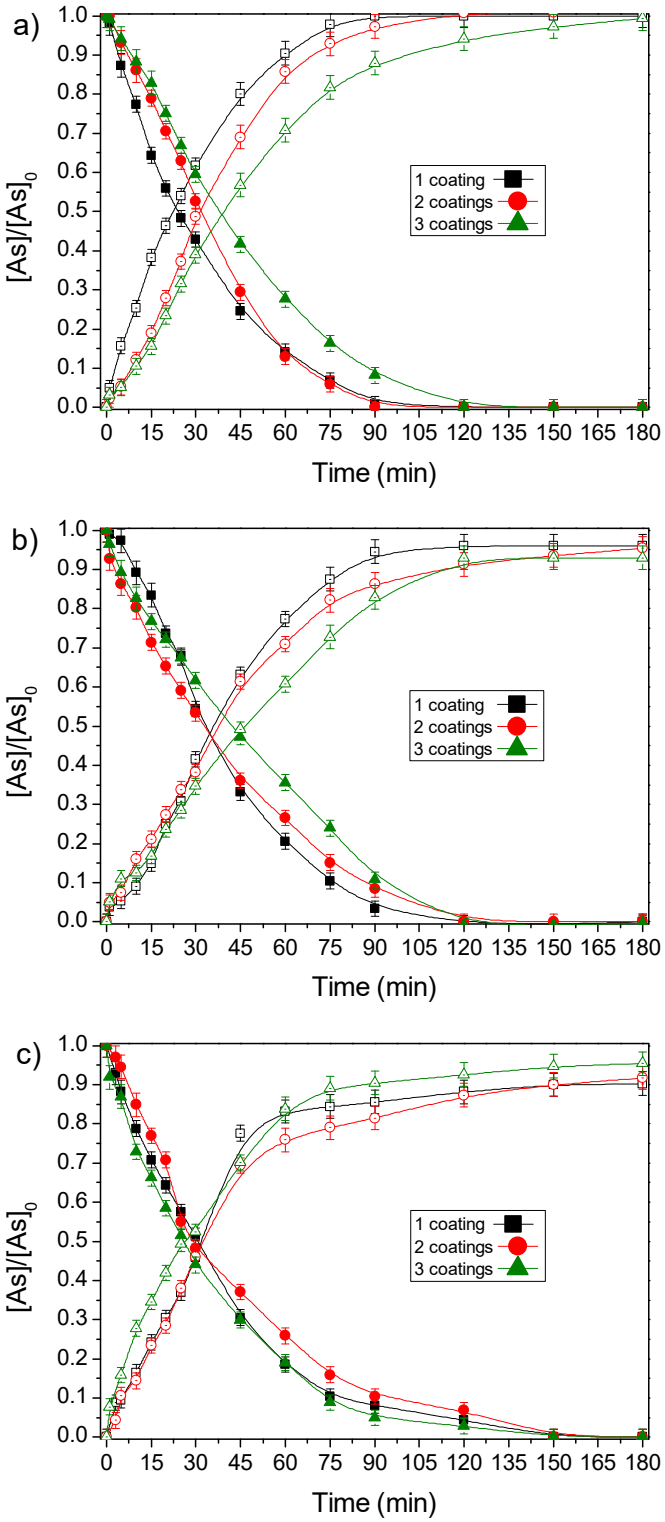

Figure 1. Photocatalytic oxidation of 10 mg L^{-1} As(III) to As(V) at pH = 9 using TiO_2 catalyst supported on glass by (a) dip coating; (b) rotational coating; and (c) sponge coating. Filled symbols: As(III); hollow symbols: As(V).

On the other hand, if the irradiation is performed from the glass support side, as it occurs in the reactor used in the present work, an optimum film thickness value will exist above which the observed pollutant conversion will decrease (Chen et al., 2001; Vezzoli et al., 2013). The given explanation is that in the latter configuration the maximum concentration of photogenerated charges and hydroxyl radicals will be close to the glass–titania interface whereas the maximum pollutant concentration-will occur at the liquid-titania interface. Therefore, above an optimum titania film thickness the reaction rate will decrease due to internal mass transfer limitations which will prevent the access of pollutants to photogenerated charge carriers (Chen et al., 2001; Vezzoli et al., 2013).

Accordingly, the diminution of the photocatalytic activity observed for titania immobilized by RC and SC methods can be explained by means of the thicker titania layers and agglomerates formed per coating cycle in each case in comparison to the dip coating procedure, preventing an optimal interaction between photogenerated charges and As(III) species from solution. Hence, as shown in Fig 1 one single TiO_2 impregnation by dip coating allowed to attain the best photocatalytic activity using the least amount of immobilized catalyst.

In all reactions As(V) was detected, confirming the photocatalytic oxidation of As(III) with the immobilized TiO_2. The mass balance of arsenic in solution was only achieved in the reactions performed with TiO_2 immobilized by DC method. In the reactions performed with TiO_2 deposited by RC and SC procedures, the final concentration of As(V) was 4% to 12% lower than the initial concentration of arsenic in solution, thus indicating the adsorption of As(V) generated species on the immobilized titania. The differences observed are in agreement with the higher amount of catalyst and the greater roughness observed for TiO_2 deposited by RC and SC methods, which provide a higher surface area for As(V) adsorption in comparison to that obtained with the DC method. However, when the amount of TiO_2 immobilized was highly increased after the third coating by the SC method, the As(V) adsorption decreased probably because some inner adsorption sites remained inaccessible.

To evaluate the mechanical stability of titania coatings attained by the three procedures, the glass cylinders were thoroughly dried after the reactions and weighted. No substantial changes were detected in the mass compared to that of the supports before reaction, thus indicating no significant detachment of catalyst during the reactions.

3.1.2. Reuse of immobilized TiO_2

Once the photocatalytic performance for the oxidation of As(III) in aqueous solution was proved for titania immobilized by DC, RC and SC, subsequent reaction cycles were carried out to evaluate the stability of the photocatalytic activity. Up to five consecutive reactions were performed with the catalyst immobilized by DC, and three uses were evaluated for TiO_2 immobilized by RC and SC. The reactions were carried out with one catalyst coating, using a fresh As(III) solution for each reaction cycle. As displayed in Figure 2, the photocatalytic activity of immobilized titania was maintained after the consecutive uses. In addition, a high reproducibility of the kinetics of As(III) removal rate was observed, especially noticeable in the reaction system with TiO_2 immobilized by DC. Moreover, no TiO_2 was detached during the reactions, so confirming the high stability of the immobilized catalyst. In the coating by the sponge method, it was observed that the extent of adsorption of As(V) formed on the catalyst decreased throughout the consecutive reuse cycles. The initial 12% percentage of As(V) adsorbed after the first use was reduced to 6% and to less than 1% after the second and third use, respectively. Nevertheless, despite this progressive deactivation of active sites for As(V) adsorption the photocatalytic activity for As(III) oxidation was preserved during the following runs. Therefore, the reuse of TiO_2 immobilized by any of the three methods (dip, rotational or sponge methods) was viable and effective. In addition, no requirement of cleaning between consecutive reaction runs was needed, thus pointing out that the procedures followed for the immobilization of titania can be taken into account for a plausible application at pilot scale operation, including continuous or semi-continuous flow processes.

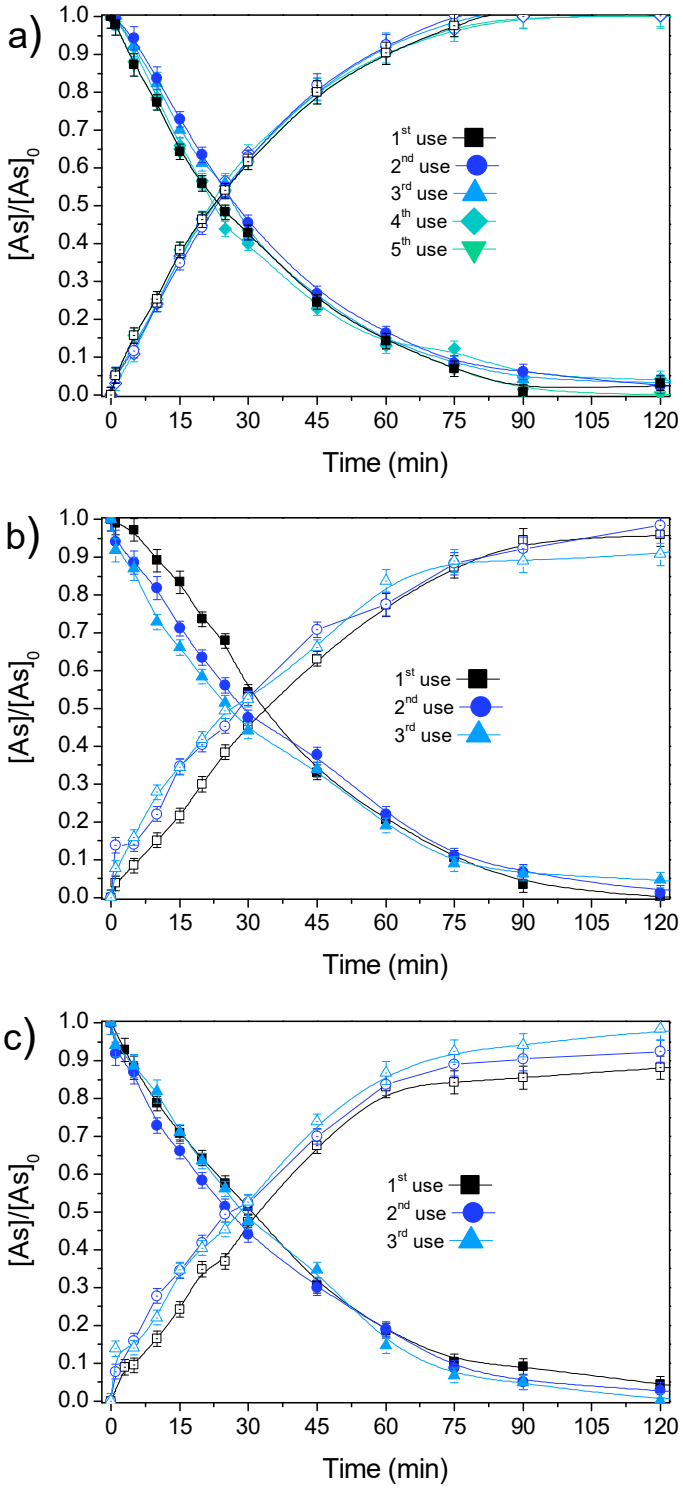

296

297 Figure 2. Reuse of single coating TiO_2 immobilized by (a) dip coating; (b) rotational coating; and

298 (c) sponge coating. Filled symbols: As(III); hollow symbols: As(V).

3.2. Effect of the addition of zero-valent iron to the immobilized TiO_2 system

In order to enhance the photocatalytic efficiency of the TiO_2 immobilized and also to achieve the complete removal of arsenic from the aqueous solution, the addition of zero-valent iron to the reaction medium was evaluated, since metallic iron was proven to have a beneficial effect in TiO_2 slurries (López-Muñoz et al., 2017; Li et al., 2010). The influence of the iron particle size was investigated by using two alternative metallic iron materials, *i.e.* commercial micro-scale and synthetized nano-scale zero-valent iron, denoted as ZVI and nZVI, respectively.

3.2.1. Characterization of ZVI and nZVI materials

Figure 3 shows TEM micrographs of nZVI material. It can be observed that the sample is composed of spherical nano-particles with an average diameter size of 55 nm (Figure 3b), which are interconnected forming a network of filaments (Figure 3a), as previously reported (Sun et al., 2006; Yan et al., 2010). This morphology is attributed to the magnetic properties of the nZVI particles (Li et al., 2010). Individual nZVI particles displayed a core-shell structure with an external surface layer (3.4 nm of average thickness) surrounding an internal core (Figure 3b). The EDX analysis revealed that the core consists of pure metallic iron which represents ca. 90% content whereas iron and oxygen were detected in the shell, which fits with the presence of iron oxides and hydroxides (Yan et al., 2010; Martin et al., 2008). On the other hand, the commercial ZVI material consists of irregular particles of metallic iron, with average size of around 45 μm, as described elsewhere (López-Muñoz et al, 2017). The BET specific surface area of synthesized nZVI, determined from N_2 sorption isotherms at 77 K was 67 $m^2 \cdot g^{-1}$, value significantly large in comparison to ZVI particles (around 10 $m^2\ g^{-1}$).

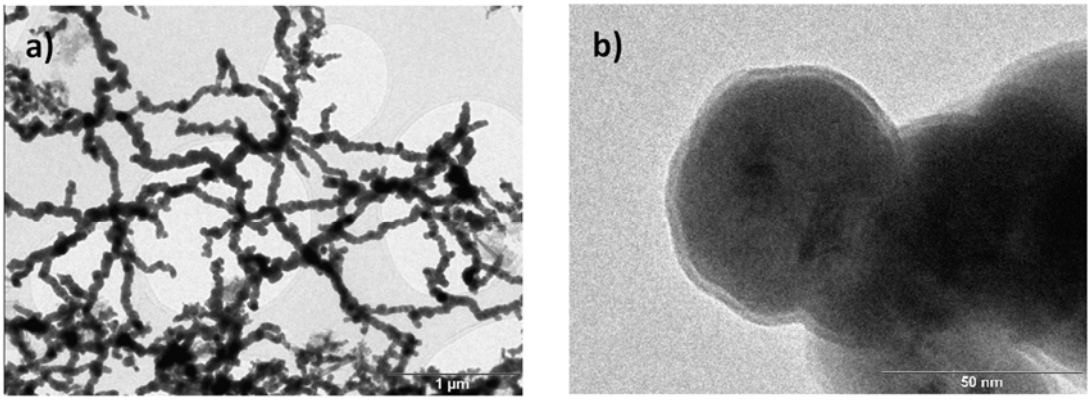

Figure 3. TEM micrographs of synthesized nZVI

The crystalline structure of the iron materials was analyzed by XRD (Figure 4). The microscale ZVI displayed three peaks with 2θ positions centered at 44.8°, 65.0° and 82.3°, attributed to the (110), (200), and (211) diffraction planes of metallic iron, α-Fe (JCPDS, No. 01-085-1410). Same diffractions were also present in the nZVI material although with broader profiles, as expected in nano-particles. An additional very small and broad reflection centered at 35.5° could be detected, probably related to the formation of iron oxides such as maghemite (γ-Fe_2O_3), wüstite (FeO), or magnetite (Fe_3O_4) whose main diffraction peaks appear at 2θ = 35.68°, 35.68°, and 35.45°, respectively, although its precise nature could not be determined from the XRD patterns.

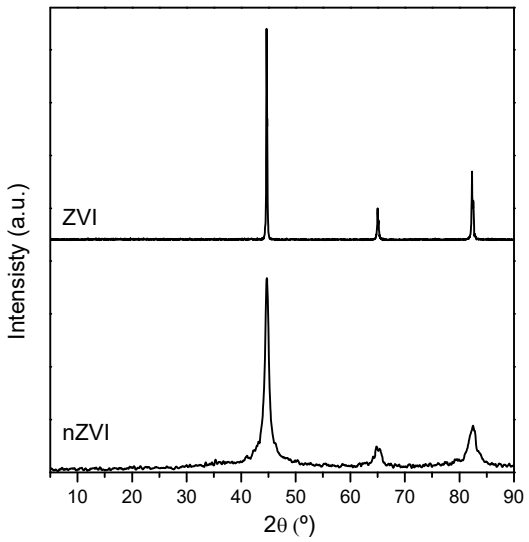

Figure 4. X-ray diffractograms of ZVI and nZVI (normalized)

Temperature programmed reduction (TPR) analysis of ZVI material did not show any reduction process confirming that the sample contains only metallic iron, in accordance to the XRD pattern. Conversely, a complex reduction profile was obtained for nZVI (Figure 5). The profile was split into three individual peaks centered at around 325 °C, 530 °C, and 730 °C, that can be related to the H_2 consumption corresponding to the stepwise reduction of iron oxides, typically γ-Fe_2O_3 (maghemite), Fe_3O_4 (magnetite), and FeO (wüstite), respectively, to yield Fe^0 (metallic iron) (Ryu et al., 2008; Bychko, 2012). Since the intensity of each reduction peak is significantly different, it can be inferred the presence of mainly magnetite with wüstite to a lesser extent and a small amount of maghemite all of which, according to the TEM micrographs, would be located on the external surface of nZVI.

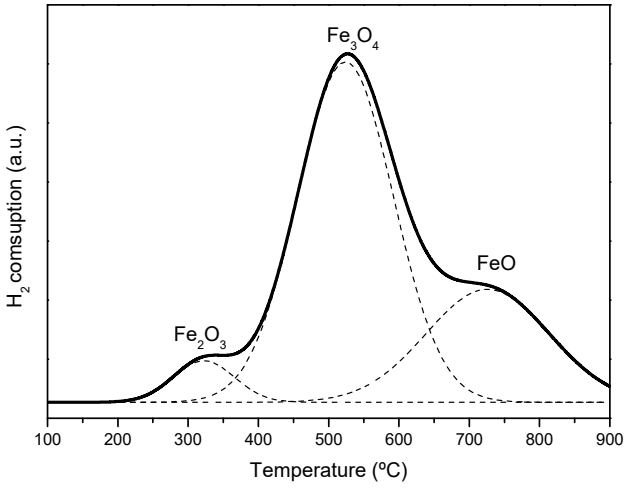

Figure 5. TPR profile of synthesized nZVI.

3.2.2. Photocatalytic reactions with titania and metallic iron

Different attempts to achieve the simultaneous immobilization of titania and iron particles on the glass support by the dip coating procedure were evaluated, with no success. The direct addition of metallic iron to the TiO_2 acid solution where the glass support should be immersed was not practicable, because the iron particles were easily oxidized at the low pH value of the titania solution. As an alternative procedure, nZVI material was sprinkled over the wet layer of fresh immobilized TiO_2 followed by subsequent drying and calcination. The nZVI particles deposited in this way exhibited no sign of oxidation, but most of the immobilized nZVI was detached from

352 the catalytic support after reaction, hence this option was also discarded. Therefore, as zero-valent
353 iron can be magnetically removed from the aqueous system, ZVI and nZVI were used under slurry
354 operation in combination with DC immobilized TiO_2. Based on previous results, the amount of
355 added zero-valent iron was fixed at 0.1 g L^{-1}.

356 Figure 6 displays the kinetic profiles for arsenic species in solution during the photocatalytic
357 reactions carried out at three different pH values (5, 7, and 9). The addition of ZVI micro-particles
358 to the immobilized TiO_2 system yielded As(III) kinetic removal profiles (Figure 6a) similar to the
359 photocatalytic reaction carried out at pH = 9 in the absence of iron (Figure 1a). No significant
360 differences in the photocatalytic rate of As(III) uptake were observed within the pH range
361 evaluated. The As(V) concentration profile throughout the reaction shows that the mass balance
362 for arsenic was achieved only at pH 9 whereas at lower pH values As(V) final concentration
363 accounted for ca. 80% As(III) initially added (Figure 6 b). This difference can be attributed to the
364 arsenate adsorption on iron oxides and hydroxides species whose formation on the ZVI micro-
365 particles would be promoted by corrosion of the iron surface as pH decreases. Nevertheless, TiO_2
366 could also contribute to the removal of As(V) since the adsorption of arsenate species on the
367 titania surface is also improved as pH decreases (López-Muñoz et al., 2017).

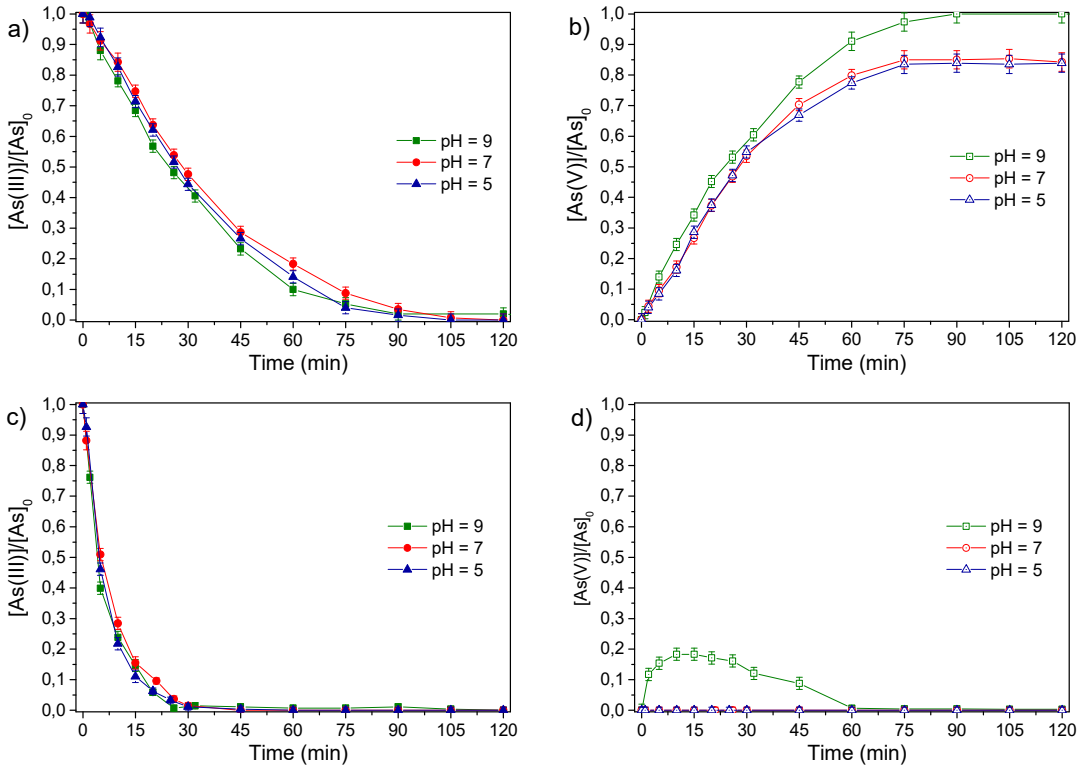

Figure 2. Influence of solution pH on 10 mg L^{-1} As(III) removal and As(V) production under UVA irradiation using immobilized TiO_2 in the presence of: commercial ZVI (a, b) and synthetized nZVI (c, d). Filled symbols: As(III); hollow symbols: As(V)

By contrast to iron microparticles, the addition of nZVI to the immobilized titania system greatly enhanced the overall uptake of arsenic from the aqueous solution (Nguyen et al., 2008). On one hand, much faster As(III) depletion kinetics were observed since the removal of As(III) was achieved within a time interval below 30 min (Figure 6.c), i.e. three times lesser than required for bare immobilized TiO_2 (Figure 1a). On the other hand, in the presence of nZVI particles a very low As(V) concentration remained in the aqueous solution after the reaction (Figure 6 d). At pH 9, the As(V) concentration firstly increased up to a 20% of the initial As(III) and then decreased to 4 µg L^{-1} after 60 min of photoreaction. At pH 7 and 5, the As(V) concentrations detected throughout the process were lower than 5 µg L^{-1}, thus indicating the positive effect of the combined system to attain in the aqueous solution a total arsenic concentration below that established by the WHO in drinking water (10 µg L^{-1}) (WHO, 2017; WHO, 2001; Jomova et. al., 2011).

Removal of pollutants by zero valent iron can proceed through four different mechanisms: reductive degradation, oxidative degradation, precipitation and adsorption (Li et al., 2006; Crane et al., 2006;). On this basis, to further investigate the role of ZVI and nZVI in the whole arsenic removal process with immobilized TiO_2, some adsorption experiments were carried out in absence of irradiation for 10 mg L^{-1} As(III) and 0.1 g L^{-1} ZVI or nZVI, as a function of time. While no adsorption of As(III) on micro-ZVI was detected at pH = 9, ca. 85% of the initial As(III) concentration was reduced after 30 min in the presence of nZVI. The decrease of pH to 5 led to some arsenite adsorption on ZVI although significantly less than obtained with nZVI, achieving after 30 min ca. 8% and 85% of As(III) removal, respectively.

The effect of pH on arsenic adsorption is governed by both the arsenic species in solution and the surface charge of the adsorbent. In aqueous solution, the predominant As(III) species at pH < 9.2 is the neutral H_3AsO_3 ($H_3AsO_3 \leftrightarrows H_2AsO_3^- + H^+$, $pK_{a1} = 9.2$). Regarding the charge of adsorbent surface, the point of zero charge (pzc) of n-ZVI has been previously reported in the 7.5-8.3 range (Kanel et al., 2005; Wu et al., 2018). Therefore, as the pH decreases from 9 to 5 the surface changes from slightly negative to positive charged. This change does not significantly affect the arsenite adsorption on nZVI since the neutral character of arsenious acid makes that electrostatic forces do not play a significant role in the interaction with the iron surface. For ZVI, the increase of As(III) adsorption by decreasing the pH from 9 to 5 can be attributed to the associated corrosion of iron particles. Indeed, the adsorption of As(III) on ZVI has been explained through the formation of complexes with the hydroxylated active groups of iron oxides (Crane et al., 2006; Kanel et al., 2005; Wu et al., 2018). In comparison to micro-ZVI, the much higher adsorption detected at any pH for n-ZVI might be attributed to the intrinsic iron oxides/hydroxides on the external surface of its particles. Moreover, due to the smaller size of nZVI particles (roughly 55 nm) and hence, their higher specific surface area, more active sites for adsorption might be available in comparison to micro ZVI.

From the above considerations, it can be inferred that adsorption must be the main process responsible for the overall diminution of As(III) concentration detected with nZVI (Fig.6c).

411 Nevertheless, as the irradiation of ZVI or nZVI particles could also promote the formation of
412 oxidizing species, the significance of the oxidative As(III) removal was further investigated.
413 Figure 7 displays the percentage of total arsenic and the speciation in As(III) and As(V) remaining
414 in solution after irradiation of 10 mg L^{-1} As(III) solutions for 30 and 60 min at pH = 9 with just
415 ZVI or nZVI particles, and each one brought together with immobilized TiO_2.

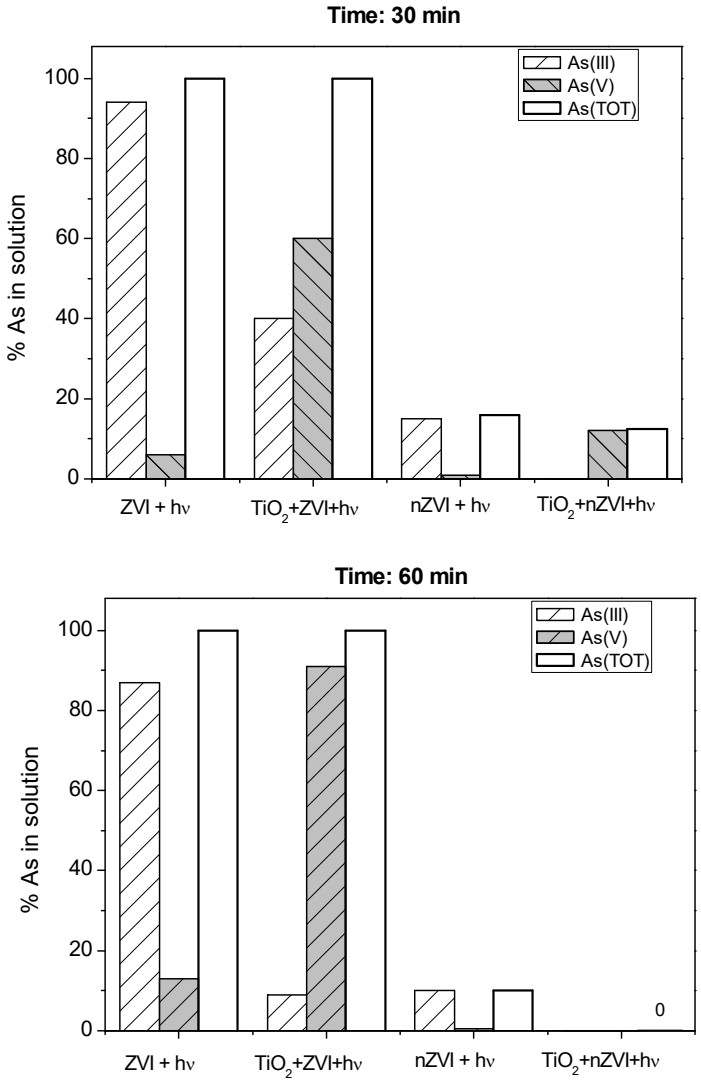

416

417 Figure 7. Percentage of As(III), As(V), and total As remaining in solution after irradiation for:
418 a) 30 min; and b) 60 min, in the presence of ZVI, nZVI, [ZVI+ TiO_2] and [nZVI+ TiO_2]

419 As it can be observed in Fig. 7, unlike the null depletion of As(III) by adsorption on ZVI at pH 9,
420 the irradiation for 30 and 60 min brought about the oxidation of a small fraction of As(III) to

As(V), ca. 5% and 12%, respectively. The achievement of mass balance for arsenic in the solution allows to discard the generation of new adsorption sites for arsenic species but points out the production under UV irradiation of oxidant species in ZVI which would be responsible for As(III) to As(V) oxidation. Regarding the nature of oxidant species formed with ZVI systems, some authors have proposed the formation of highly reactive hydroxyl radicals at low pH values whereas, above pH 5 less oxidizing intermediates such as Fe(IV) species might prevail (Katsoyannis et al., 2008). Therefore, considering the effective production of ROS under UV irradiation of TiO_2 in the pH range 5 to 9, the contribution of ZVI to As(III) oxidation should be quite scarce, in agreement with the results obtained with the [TiO_2+ZVI] system (Fig. 6 and 7).

By contrast to ZVI, a much higher decrease of As(III) concentration was detected with nZVI after 30 and 60 min of irradiation (Fig. 7), ca. 87 and 92 %, respectively, values slightly higher than obtained by adsorption in the dark (85%). Moreover, the mass balance of arsenic in the aqueous solution was not attained with nZVI. These results could be related to both an enhancement of As(III) oxidation by UV-generated oxidant species and/or the improvement of As(III) and As(V) adsorption due to the increase of the external layer of iron oxides/hydroxides species formed by the UV-induced corrosion of the nZVI surface (Morgada et al., 20115; López-Muñoz et al., 2017; Ramos Guivar et al., 2018).

Compared to the individual system, a greater removal of As(III) (> 99.9%) was attained after 30 min of irradiation with the [TiO_2+nZVI] system. In addition, with nZVI most arsenic remaining in solution after irradiation was present as As(III) while only As(V) was detected with the [TiO_2+nZVI] system, thus clearly indicating the much better efficiency of titania to achieve the oxidation of As(III) under UV-irradiation. Moreover, it should be noticed that the uptake of total arsenic, i.e. As(III)+As(V), to a concentration in solution below the detection limit could only be accomplished with the [TiO_2+nZVI] system, after 60 min of irradiation.

Regarding the concentration profile of As(V) species (Figures 6d and 7), it can be inferred that the affinity of the iron surface for As(V) increased as pH decreased. In addition, the extent of As(V) adsorption is much greater on nZVI compared to ZVI. The results prove that once As(III)

448 is oxidized to As(V) in the photocatalytic reaction, arsenate species could be immediately
449 removed by adsorption on nZVI with increasing efficiency as pH decreases. Acid dissociation
450 constants of H_3AsO_4 are 2.23, 6.94 and 11.50, therefore in the 9-5 pH range the main arsenate
451 species in solution are the anionic $H_2AsO_4^-$ and $HAsO_4^{2-}$ which are better adsorbed as pH
452 decreases due to the increasing positive charge of the iron surface. Likewise, according to its
453 isoelectric point (6.8), TiO_2 would also contribute to the As(V) adsorption as pH decreases (Singh
454 et al., 2013; Shan et al., 2010).

455 Finally, the spent nZVI was analyzed by TEM microscopy to evaluate the modifications in the
456 structure induced throughout the reactions. The micrographs of nZVI recovered after the reaction
457 with immobilized TiO_2 at pH 7 showed a broadening of the iron oxides/hydroxides shell around
458 the metallic iron core, with the formation of disordered agglomeration of particles (Figure 8).
459 According to the electron diffraction analysis of these particles, they mainly consisted of wustite
460 (FeO) (inset in Figure 8 b). Besides the Fe and O content (ca. 75% and 20% wt., respectively)
461 consistent with the presence of metallic iron and iron oxides/hydroxides, the EDX analysis
462 revealed the presence of arsenic, ca. 8% by weight of the composition of the particles, which
463 confirms the removal of arsenic from the solution by adsorption on nZVI.

464 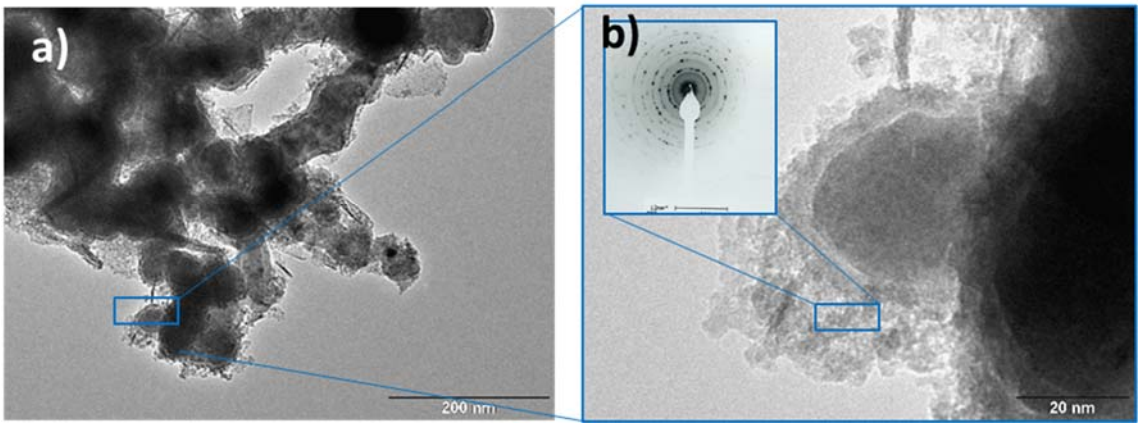

465 Figure 8. TEM micrographs of the nZVI material recovered after the photocatalytic reaction with
466 immobilized TiO_2 + 0.1 g L^{-1} nZVI at pH 9. Inset in b) displays the electron diffraction analysis
467 of the selected zone.

4. Conclusions

Photocatalytic oxidation of As(III) to As(V) in aqueous solution could successfully accomplished by titania immobilized on a glass support. The three immobilization procedures investigated allowed to attain the complete As(III) oxidation (initial concentration of 10 mg L^{-1}) but dip coating procedure was the most effective as it showed the faster kinetics. The stability of immobilized titania was proven as no loss photocatalytic activity for aqueous As(III) oxidation was detected for the three settings along consecutive cycles, up to five.

The addition of microscale ZVI to the photocatalytic TiO_2 system did not bring about significant changes in the kinetics for As(III) oxidation at the three pH values investigated, i.e., 5, 7 and 9 what can be explained considering a limited corrosion of the iron surface that, on one side leads to the production of less oxidant species that TiO_2 and on the other, does not provide a great number of sites for As(V) adsorption. On the contrary, the addition of nZVI to the immobilized titania setting greatly enhanced the kinetics for As(III) depletion and also the removal of As(V) from the solution to concentrations below 10 μg L^{-1}. This result could be related to the increase of the external layer of oxides and hydroxides of iron particles which provides available sites for As(III) and As(V) adsorption and also, the formation of additional ROS species under UV irradiation. The [nZVI+immobilized-TiO_2] system can be then a suitable option for the treatment of arsenic polluted water.

Acknowledgements

The authors gratefully acknowledge the financial support of the Spanish State Research Agency (AEI) and the Spanish Ministry of Science, Innovation and Universities through the projects CTM2015-72910-EX, CALYPSOLATECWATER (RTI2018-097997-B-C33) and pre-doctoral grant BES-2013 064621 and Comunidad de Madrid through the program REMTAVARES (P2018/EMT-4341).

492 **5. References**

493 Abdul, K.S.M., Jayasinghe, S.S., Chandana, E.P.S., Jayasumana, C., De Silva, P.M.C.S., 2015.
494 Arsenic and human health effects: A review. Environ. Toxicol. Pharmacol. 40, 828–846.

495 Balasubramanian, G., Dionysiou, D.D., Suidan, M.T., Baudin, I., Laîné, J.-M., 2004. Evaluating
496 the activities of immobilized TiO_2 powder films for the photocatalytic degradation of organic
497 contaminants in water. Appl. Catal. B Environ. 47, 73–84.

498 Bhaumik, M., Noubactep, C., Gupta, V.K., McCrindle, R.I., Maity, A., 2015. Polyaniline/Fe^0
499 composite nanofibers: An excellent adsorbent for the removal of arsenic from aqueous solutions.
500 Chem. Eng. J. 271, 135–146.

501 Bhowmick, S., Chakraborty, S., Mondal, P., Van Renterghem, W., Van den Berghe, S., Roman-
502 Ross G., Chatterjee, D., Iglesias, M., 2014. Montmorillonite-supported nanoscale zero-valent iron
503 for removal of arsenic from aqueous solution: Kinetics and mechanism. Chem. Eng. J. 243, 14–
504 23.

505 Brunauer, P., Emmett, H., Teller, E., 1938. Adsorption of Gases in Multimolecular Layers. J. Am.
506 Chem. Soc. 60, 309–319.

507 Bychko, I., 2012. TPR study of core-shell Fe@Fe3O4 nanoparticles supported on activated
508 carbon and carbon nanotubes. Adv. Mater. Phys. Chem. 02, 17–22.

509 Chen, D., Li, F., Ray, A.K., 2001. External and internal mass transfer effect on photocatalytic
510 degradation. Catal. Today. 66, 475–485.

511 Chen, Y., Dionysiou, D. D., 2006. TiO_2 photocatalytic films on stainless steel: The role of
512 Degussa P-25 in modified sol–gel methods. Appl. Catal. B Environ. 62, 255–264.

513 Choi, W., Yeo, J., Ryu, J., Tachikawa, T., Majima, T., 2010. Photocatalytic oxidation mechanism
514 of As(III) on TiO_2: Unique role of As(III) as a charge recombinant species. Environ. Sci. Technol.
515 44, 9099–9104.

516 Crane, R.A., Scott, T.B., 2012. Nanoscale zero-valent iron: future prospects for an emerging water
517 treatment technology. J. Hazard. Mater. 211–212, 112–125.

518 Dijkstra, M.F.J., Michorius, A., Buwalda, H., Panneman, H.J., Winkelman, J.G.M., Beenackers,
519 A.A.C.M., 2001. Comparison of the efficiency of immobilized and suspended systems in
520 photocatalytic degradation. Catal. Today. 66, 487–494.

521 Dutta, P.K., Pehkonen, S.O., Sharma, V.K., Ray, A.K., 2005. Photocatalytic oxidation of
522 arsenic(III): evidence of hydroxyl radicals. Environ. Sci. Technol. 39, 1827–1834.

523 El-Kalliny, A.S., Ahmed, S.F., Rietveld, L.C., Appel, P.W., 2014. Immobilized photocatalyst
524 structure assuring optimal light distribution in a solar reactor. Drink. Water Eng. Sci. Discuss. 7,
525 59–94.

526 Falk, G.S., Borlaf, M., López-Muñoz, M. J., Fariñas, J. C., Rodrigues Neto, J. B., Moreno, R.,
527 2018. Microwave-assisted synthesis of TiO_2 nanoparticles: photocatalytic activity of powders and
528 thin films. J. Nanopart. Res. 20(2) art. no. 23.

529 Ferguson, M.A., Hoffmann, M.R., Hering, J.G., 2005. TiO_2-photocatalyzed As(III) oxidation in
530 aqueous suspensions: reaction kinetics and effects of adsorption. Environ. Sci. Technol. 39, 1880–
531 1886.

532 Jomova, K., Jenisova, Z., Feszterova, M., Baros, S., Liska, J., Hudecova, D., Rhodes, C.J., Valko,
533 M., 2011. Arsenic: Toxicity, oxidative stress and human disease. J. Appl. Toxicol. 31, 95–107.

534 Kanel, S.R., Manning, B., Charlet, L., Choi, H., 2005. Removal of Arsenic (III) from
535 Groundwater by Nanoscale Zero-Valent Iron. Environ. Sci. Technol. 39, 1291–1298.

536 Katsoyannis, I., Ruettimann, T., Hug, S.J., 2008. pH Dependence of Fenton Reagent Generation
537 and As(III) Oxidation and Removal by Corrosion of Zero Valent Iron in Aerated Water. Environ.
538 Sci. Technol. 42,7424–7430.

539 Li, L., Fan, M., Brown, R.C., Van, J.H., Wang, J., Wang, W., Song, Y., 2010. Synthesis,
540 Properties and Environmental Applications of Nanoscale Iron-Based Materials: A Review.
541 Environ. Sci. Technol. 36, 405–431.

542 Li, X., Elliott, D.W., Zhang, W., 2006. Zero-Valent Iron Nanoparticles for Abatement of
543 Environmental Pollutants: Materials and Engineering Aspects. Crit. Rev. Solid State Mater. Sci.
544 31, 111-122.

545 López-Muñoz, M.J., Arencibia, A., Segura, Y., Raez, J.M., 2017. Removal of As(III) from
546 aqueous solutions through simultaneous photocatalytic oxidation and adsorption by TiO_2 and
547 zero-valent iron. Catal. Today. 280, 149–154.

548 López-Muñoz, M.J., Revilla, A., Alcalde, G. Brookite, 2015. TiO_2-based materials: Synthesis and
549 photocatalytic performance in oxidation of methyl orange and As(III) in aqueous suspensions.
550 Catal. Today. 240, 138–145.

551 Manassero, A., Satuf, M.L., Alfano, O.M., 2017. Photocatalytic reactors with suspended and
552 immobilized TiO_2: Comparative efficiency evaluation. Chem. Eng. J. 326, 29–36.

553 Martin, J. E., Herzing, A.A., Yan, W., Li, X.-q., Koel, B. E., Kiely, C. J., Zhang, W.-x., 2008.
554 Determination of the Oxide Layer Thickness in Core-Shell Zerovalent Iron Nanoparticles.
555 Langmuir, 24, 4329-4334.

556 Marugán, J., López-Muñoz, M.J., Fernández-Ibáñez, P., Malato, S., 2016. Solar photocatalysis:
557 Fundamentals, reactors and applications. RSC Energy Environ. Ser., The Royal Society of
558 Chemistry, Cambridge, pp. 92–129.

559 Morgada, M.E., Levy, I.K., Salomone, V., Farías, S.S., López, G., Litter, M.I., 2009. Arsenic (V)
560 removal with nanoparticulate zerovalent iron: Effect of UV light and humic acids. Catal. Today.
561 143, 261–268.

562 Nguyen, T.V., Vigneswaran, S., Ngo, H.H., Kandasamy, J., Choi, H.C., 2008. Arsenic removal
563 by photo-catalysis hybrid system. Sep. Purif. Technol. 61, 44–50.

564 Ponder, S.M., Darab, J.G., Mallouk, T.E., 2000. Remediation of Cr(VI) and Pb(II) aqueous
565 solutions using supported nanoscale zero-valent iron. Environ. Sci. Technol. 34, 2564–2569.

566 Ramos Guivar, J.A., Bustamante, A. D., Gonzalez, J.C., Sanches, E.A., Morales, M.A., Raez,
567 J.M., López-Muñoz, M.J., Arencibia, A., 2018. Adsorption of arsenite and arsenate on binary and
568 ternary magnetic nanocomposites with high iron oxide content. Appl. Surf. Sci. 454, 87-100.

569 Ryu, J., Suh, D., Park, J. Y.K., Suh, Y.W., 2008. Effect of reduction temperature on the
570 preparation of zero-valent iron aerogels for trichloroethylene dechlorination. Korean J. Chem.
571 Eng. 25, 1377–1384.

572 Shan, A.Y., Ghazi, T.I.M., Rashid, S.A., 2010. Immobilisation of titanium dioxide onto
573 supporting materials in heterogeneous photocatalysis: A review. Appl. Catal. A Gen. 389, 1–8.

574 Shankar, S., Shanker, U., Shikha, 2014. Arsenic contamination of groundwater: A review of
575 sources, prevalence, health risks, and strategies for mitigation. Sci. World J. 2014, 304524.

576 Sharma, V.K., Sohn, M., 2009. Aquatic arsenic: Toxicity, speciation, transformations, and
577 remediation. Environ. Int. 35, 743–759.

578 Singh, S., Singh, P.K., 2013. Polymer-supported titanium dioxide photocatalysts for
579 environmental remediation: A review. Appl. Catal. A Gen. 462-463, 178–195.

580 Sorlini, S., Gialdini, F., 2010. Conventional oxidation treatments for the removal of arsenic with
581 chlorine dioxide, hypochlorite, potassium permanganate and monochloramine. Water Res. 44,
582 5653–5659.

583 Su, C., Puls, R.W., 2001. Arsenate and arsenite removal by zerovalent iron: Kinetics, redox
584 transformation, and implications for in situ groundwater remediation. Environ. Sci. Technol. 35,
585 1487–1492.

586 Sun, Y.-P., Li, X., Cao, J., Zhang, W., Wang, H.P., 2006. Characterization of zero-valent iron
587 nanoparticles. Adv. Colloid Interface Sci. 120, 47–56.

588 Van Grieken, R., Marugán, J., Sordo, C., Pablos, C., 2009. Comparison of the photocatalytic
589 disinfection of E. coli suspensions in slurry, wall and fixed-bed reactors. Catal. Today. 144, 48–
590 54.

591 Vezzoli, M., Farrell, T., Baker, A., Psaltis, S., Martens, W.N., Bell, J.M., 2013. Optimal catalyst
592 thickness in titanium dioxide fixed film reactors: Mathematical modelling and experimental
593 validation. Chem. Eng. J. 234, 57–65.

594 World Health Organization, Guidelines for drinking-water quality: fourth edition incorporating
595 the first addendum. Geneva: World Health Organization; 2017. Licence: CC BY-NC-SA 3.0 IGO.
596 ISBN 978-92-4-154995-0

597 World Health Organization, United Nations Synthesis Report on Arsenic in Drinking-Water
598 Chapter 1. Source and behaviour of arsenic in natural waters, Geneva, 2001.

599 Wu, D., Peng, S., Yan, K., Shao, B., Feng, Y., Zhang, Y., 2018. Enhanced As(III) Sequestration
600 Using Sulfide-Modified Nano-Scale Zero-Valent Iron with a Characteristic Core–Shell Structure:
601 Sulfidation and As Distribution. ACS Sustain. Chem. Eng. 6, 3039–3048.

602 Yan, W., Herzing, A.A., Kiely, C.J., Zhang, W.X., 2010. Nanoscale zero-valent iron (nZVI):
603 Aspects of the core-shell structure and reactions with inorganic species in water. J. Contam.
604 Hydrol. 118, 96–104.

605 Yoon, S.H., Oh, S.E., Yang, J.E., Lee, J.H., Lee, M., Yu, S., Pak, D., 2009.TiO_2 photocatalytic
606 oxidation mechanism of As(III). Environ. Sci. Technol. 43, 864–869.

607 Yu, L., Peng, X., Ni, F., Li, J., Wang, D., Luan, Z., 2013. Arsenite removal from aqueous solutions
608 by γ-Fe_2O_3–TiO_2 magnetic nanoparticles through simultaneous photocatalytic oxidation and
609 adsorption. J. Hazard. Mater. 246, 10–17.